Phonon localization in cubic GaN/AlN superlattices

A.D. Rodrigues [a], M.P.F. de Godoy [a,], C. Mietze [b], D.J. As [b]

[a] *Departamento de Física, Universidade Federal de São Carlos – UFSCar, 13565-905, São Carlos, SP, Brazil*
[b] *Department Physik, Universität Paderborn, Warburger Str. 100, D-33098 Paderborn, Germany*

ARTICLE INFO

ABSTRACT

To enhance the device's performance a better understanding of the confinement of polar optical-phonons in the heterostructures should be achieved. In this work, we investigated a set of three cubic GaN/AlN superlattices (SL) grown by plasma-assisted Molecular Beam Epitaxy (MBE) on 3C–SiC substrates by structural and optical measurements. Reciprocal Space Mapping (RSM) at the (113) reflections revealed the SL satellite peaks and the strain in the structures as well photoluminescence spectra evidence the quantum confinement. Different line broadenings in the Raman spectra measured in each heterostructure indicate that the longitudinal optical phonons of GaN describe different localization lengths. Through the application of the spatial correlation model we have quantified the localization length of these phonons and established a correlation with the GaN layer thicknesses. For the first time it is presented localized optical phonons (LO) in cubic GaN layers.

© 2014 Elsevier Ltd. All rights reserved.

1. Introduction

Wide-band gap heterostructures based on group-III nitrides received great interest due to the applications in optoelectronic devices in the ultraviolet and infrared spectral ranges. Usually, the development of these devices employs the hexagonal phase of GaN which has the disadvantage to produce built-in electric fields. This is a factor that limits the performance of optoelectronics due to the induced quantum-confined Stark Effect. However, the high crystal symmetry of metastable cubic phase of GaN and AlN has no polarization field in (001) growth direction. Many efforts have been done to develop high crystal quality nitrides, reducing the surface roughness of layers and optimizing the hetero-interface and structural quality of multilayer stacks. The ability to fabricate such nanostructures based on III-nitrides has allowed the exploration of its electronic properties in photodetectors and field effect transistors [1–3]. Besides the quantum confinement of charges due to nanoscale dimensionality, the confinement or localization of acoustic and optical phonons leads to interesting changes in the phonon spectra [4]. The localization of phonons allow phonon-assisted intersubband transitions in step quantum well structures [5] and it opens the possibility to use this feature to intersubbands lasers [6]. This could be done by designing the first excited states in a quantum well with separation energies lower than the longitudinal optical phonon energy. This configuration strongly reduces the scattering to lower energy levels and it can be employed to achieve a population inversion in this structure. Such application of phonon localized effects is one of the most important applications of confined-phonon physics [7–10].

Theoretical studies on hexagonal GaN/AlN superlattices (SL) have already been reported [9]. Recently, Davydov et al. [11] reported the first observation of $A_1(LO)$ phonons confined to AlN layer in short-period GaN/AlN SL with hexagonal symmetry. A remarkable consequence of the phonon confinement in the Raman spectrum is the development of a strong asymmetry on the optical phonon line shape. However, the asymmetric shape of Raman peaks could also be attributed to a distribution of tensile strain in multilayer stacked structures. Thus, better understanding of phonon localization in cubic III-nitrides is aimed.

In this work we study the characteristics of metastable cubic phase AlN/GaN superlattices by structural and optical techniques. We analyzed a set of three GaN/AlN cubic superlattices (SL) grown by plasma-assisted Molecular Beam Epitaxy (MBE) on 3C–SiC substrates. The optimal stoichiometry conditions for the epitaxial growth and the thickness of layers were monitored by in-situ reflection high energy electron diffraction (RHEED). Reciprocal Space Mapping (RSM) measured by high resolution X-ray diffraction (HRXRD) at the (113) reflections revealed the SL satellite peaks and the strain in the structures. Photoluminescence spectra of the SL evidence the quantum confinement, as compared to bulk free-exciton emission of cubic GaN. Localized optical phonons (LO) in Raman spectra were observed in GaN layers in direct correlation with the layer thickness for the first time.

2. Materials and methods

The samples were grown by plasma-assisted molecular beam epitaxy at a temperature of 720 °C which favors the growth of metastable nitrides cubic phase. A reference bulk c-GaN sample

E-mail address: mgodoy@ufscar.br (M.P.F. de Godoy).

was grown after 8 nm AlN buffer layer on 3C–SiC (001) substrate. During the growth of c-GaN layers, the optimum condition for low roughness of 1 monolayer (ML) of free Ga is employed [12]. Three SL samples consisting of 100 periods AlN/GaN were grown directly on 3C–SiC substrate. The AlN barrier thickness was 2 nm constant for all samples and the GaN layers of SL were 4, 7 and 10 nm, respectively. Therefore, they are labeled SL4, SL7 and SL10. The cubic AlN/GaN superlattices were characterized by High Resolution X-Ray Diffraction (HRXRD), photoluminescence (PL) and Raman spectroscopy. HRXRD was performed using a Panalytical X´Pert diffractometer. For diffraction the copper $K_{\alpha 1}$ line with a wavelength of 1.54056 Å was used, which was separated from the X-ray spectrum by a hybrid monochromator. The hybrid monochromator consists of a parallelizing mirror and a 4 bounce germanium (220) crystal monochromator which blocks the $K_{\alpha 2}$ line and reaches a beam divergence of $\Delta\Theta = 47''$. For PL measurements, the 325 nm line of a HeCd laser was employed as excitation source and the detection was performed by a 0.5 m Andor spectrometer equipped with a Si CCD. Raman spectra were recorded by a Jobin-Yvon triple grating spectrometer using microscope facilities. In order to suppress the photoluminescence of the 3C–SiC substrate and its contribution to the Raman spectra, we employed the line 568.2 nm of an Ar^+/Kr^+ laser as excitation source. The spectra were collected in backscattering geometry at room temperature.

3. Results

3.1. Structural and optical characterization

By XRD diffraction, the strain in the superlattice samples was investigated by reciprocal space maps (RSMs) of the asymmetrical (113) reflection. In Fig. 1 the RSMs of the three different superlattice structures are depicted. In all three maps we see that the c-AlN layers are not fully strained on c-GaN. From the position of the satellites peaks associated with the superlattices we conclude that the superlattice structure has formed an average lattice constant between full relaxed c-AlN and c-GaN, meaning that the c-AlN layer are partially relaxed while the GaN is partially strained. Besides the experimental data (gray contours) the theoretical positions of cubic GaN, relaxed cubic AlN and cubic AlN strained on cubic GaN are marked with red squares. The experimental value of $q_\parallel$ of the SL satellites (indicated by the full vertical red line) is between the theoretical value of c-GaN and c-AlN, which is an indicator for the strain status of the layers as mentioned above. Since the lattice parameter from 3C–SiC substrate (4.35 Å) is near the c-AlN (4.38 Å), while c-GaN is 4.52 Å, there is a tendency to relax to the GaN lattice parameter when such layer is thicker than the AlN ones. However, we observed a similar relaxation for all SL, namely 2.0%, 2.3%, and 1.7% for SL10, SL7 and SL4 respectively, which can be evaluated by the definition $\varepsilon = (q_\parallel(SL) - q_\parallel(AlN))/q_\parallel(AlN)$. The amount of hexagonal group III-nitride inclusions have also been checked by performing RSM around the symmetric GaN (002) or AlN (002) reflections. From the intensity ratio between cubic (002) to the hexagonal (1011) reflections, the amount of hexagonal inclusions in the reference sample has been determined to be below 0.3% [13].

The PL spectra in Fig. 2 show the emission of SL at low temperature (right) and room temperature (left) due to the quantum confinement as compared to bulk free-exciton emission of c-GaN. As expected, in absence of a polarization field due to cubic symmetry, the peak emission energy increases as QW thickness decreases [14]. The full width at half maximum (FWHM) is around 90–100 meV due to structural defects.
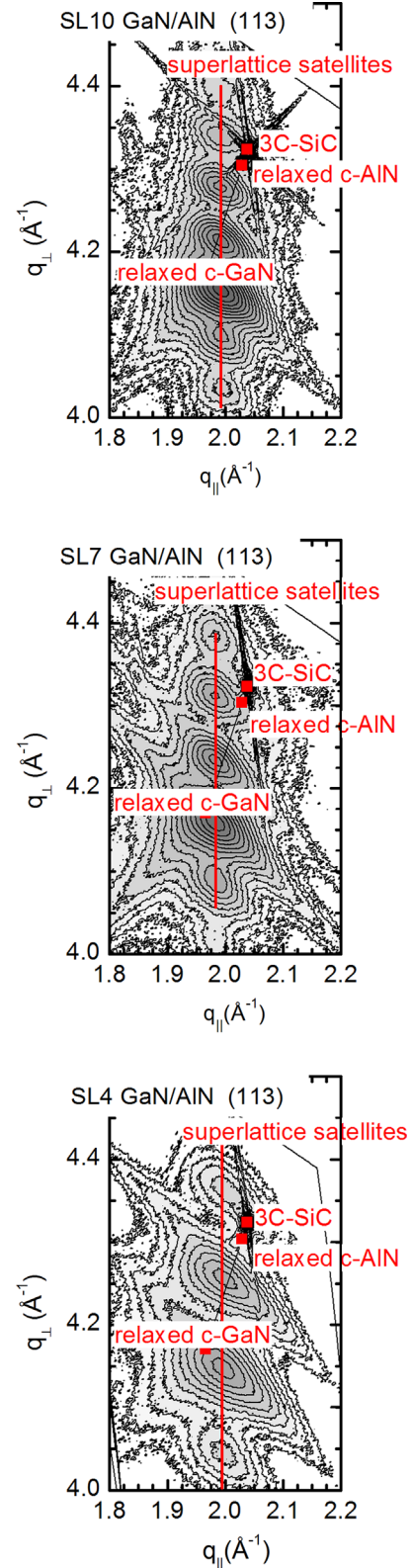

Fig. 1. (Color online) HRXRD reciprocal map at (113) direction for GaN/AlN superlattices with GaN thickness of 10, 7 and 4 nm. The AlN barrier thickness was 2 nm. It shows the satellites peaks referent to the superlattices between full relaxed c-AlN and c-GaN.

3.2. Raman measurements

As we can observe from Fig. 3a, there are three representative bands in SL Raman spectra. The first one, centered at 560 cm^{-1} and
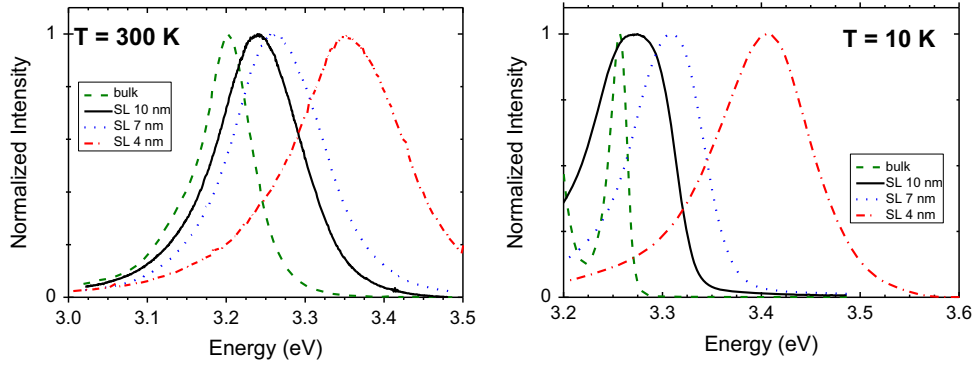
Fig. 2. (Color online) PL spectra at low (right) and room temperatures (left) of bulk cubic GaN and GaN/AlN superlattices with GaN thickness of 4, 7 and 10 nm, respectively and an AlN barrier thickness of 2 nm.

named TO_{GaN}, can be attributed to the density of states of GaN-like TO phonons, activated by disorder. It also appears in the GaN bulk. We observe that the band related to GaN-like TO phonons in SL are found to be blue shifted as respected to bulk, due to compressive strain in the GaN layers. The spectral features at 635 cm^{-1} are attributed to the TO phonons in AlN (TO_{AlN}), red shifted due to the tensile strain in the direction perpendicular to growth axis. The peak at 741 cm^{-1} is attributed to the LO phonons in the GaN layers, labeled LO_{GaN}. The absence of c-GaN buffer layers in SL samples intends to avoid superposition of bulk LO_{GaN} lines in the Raman spectra. It can be noticed that the LO_{GaN} peaks in the SL spectra present downward asymmetric shapes when compared to the same spectral feature measured in the bulk c-GaN. Modifications in both, the shape and central position of Raman lines, can be produced by the presence of strain and quantum confinement in some structures. In order to understand the correct nature of the asymmetric shape of the LO_{GaN} lines, and discuss the mechanism of localization of phonon wavefunctions, we have applied the spatial correlation model [15]. In this model, the emergence of an asymmetric shape in a peak is generated by the contribution of a density of phonon states to the Raman signal. If the vibrations have a finite coherence length L_C, an enhancement in the momentum uncertainty of the oscillations promotes a relaxation in the selection rule for the momentum conservation, allowing excitations with $q > 0$ to contribute to the Raman intensity, with energies given by their dispersion relations. Fig. 3b shows a representative schema of this mechanism, in which, since we have considered a negative dispersion relation, the contribution of phonons with wave numbers below the center of the Brillouin zone (Γ point) provokes a downward asymmetric shape in the Raman line. The peak broadening will be dependent on the phonons coherence length in inverse proportion. In the presence of strong phonon localization, the Raman intensity will be given by

$$I(\omega)\alpha \int \exp\left(-\frac{q^2 L_C^2}{4}\right)\frac{d^3 q}{[\omega - \omega(q)]^2 + \left(\frac{\Gamma}{2}\right)^2} \tag{1}$$

where q is the phonon wavevector, $\omega(q)$ is the phonon dispersion curve, Γ is the natural linewidth and L_C is the coherence length of the LO phonons in the considered layer. Since the density of states of optical phonons in GaN and AlN exist in different energy ranges, a vibrational mode with typical energy of the GaN optical vibrations cannot occur in AlN. For this fact, optical phonons originated in the GaN layers are prevented to propagate through the AlN adjacent layers, imposing a spatial confinement of the phonons to the well layers. As can be noticed in Fig. 3a, the SL with thinner GaN layers present broader LO_{GaN} lines, probably as a result of more effective phonon localization inside the wells. To verify this assumption we have quantified the LO_{GaN} phonons localization length. In this

procedure the theoretical Raman spectra for each SL has been calculated using Eq. (1) for the Raman intensity on LO_{GaN} spectral range. The phonon dispersion curve $\omega(q)$ needed for these calculations was taken from [16]. By fitting the theoretical to the experimental spectra we have determined the LO_{GaN} phonon localization length in our structures. Fig. 3c shows the experimental (thin black lines) and the theoretical (gray lines) Raman spectra for each sample in the interval of longitudinal optical vibration of GaN. The dashed lines present the components of the theoretical spectra calculated by Eq. (1). The obtained values for SL10 and SL7, shown in Fig. 3c, are in good agreement with the nominal GaN layers thicknesses, which confirms a good achievement of layer dimensions during the samples growth. However, the phonon localization length of 5.5 nm for SL4 is slightly larger compared to that expected for the superlattice with 4 nm thick GaN layers. This result will be discussed in more detail further below. For L_C values higher than 40 nm the Raman intensity calculated by Eq. (1) results in a symmetric peak, as the same way to those measured in bulk materials, in which the vibrational modes propagate through the whole material, describing an infinite coherence length. The selection rule for the momentum conservation is preserved and the phonons with wave vectors far from Brillouin zone center do not contribute significantly to the Raman intensity. Since no modification in the line shape can be noticed for vibrational coherence length larger than 40 nm, this value can be assumed as the upper limit for the determination of phonons localization by this method. Further referring to Fig. 3b, the dashed line of LO_{GaN} mode of the film sample presents a well-defined symmetric shape, indicating the absence of phonon confinement effects within the above mentioned limit, as a consequence of long-range crystalline order in the GaN film. The difference between the coherence length of the LO_{GaN} phonons obtained by our Raman analyses and the nominal thickness of the wells in sample SL4 can be attributed to the presence of non-abrupt interfaces in this sample. Remembering that we are dealing with superlattices grown directly on SiC substrate, i.e., no buffer layer was deposited between the substrate and the periodic structure, fluctuations in the substrate morphology can be reproduced during the growth process, provoking an uncertainty in the well thickness determination. Even for cubic superlattices grown on buffer layers, the resulting interface roughness can be in the order of 1–2 ML [17]. So, the obtained length of the phonon localization for the SL4 sample is in agreement with the uncertainty interval expected for the well thickness, considering the roughness of the two interfaces of each well. The presence of a significant roughness in interfaces is corroborated by the PL spectra shown in Fig. 2. The charge carriers in the wells of referred SL are confined by distances with uncertainty determined by the interfaces roughness. The fluctuations in the length of the quantum confinement lead to a broadening of the electronic state energies, resulting in an increasing in the FWHM of the PL peak in comparison
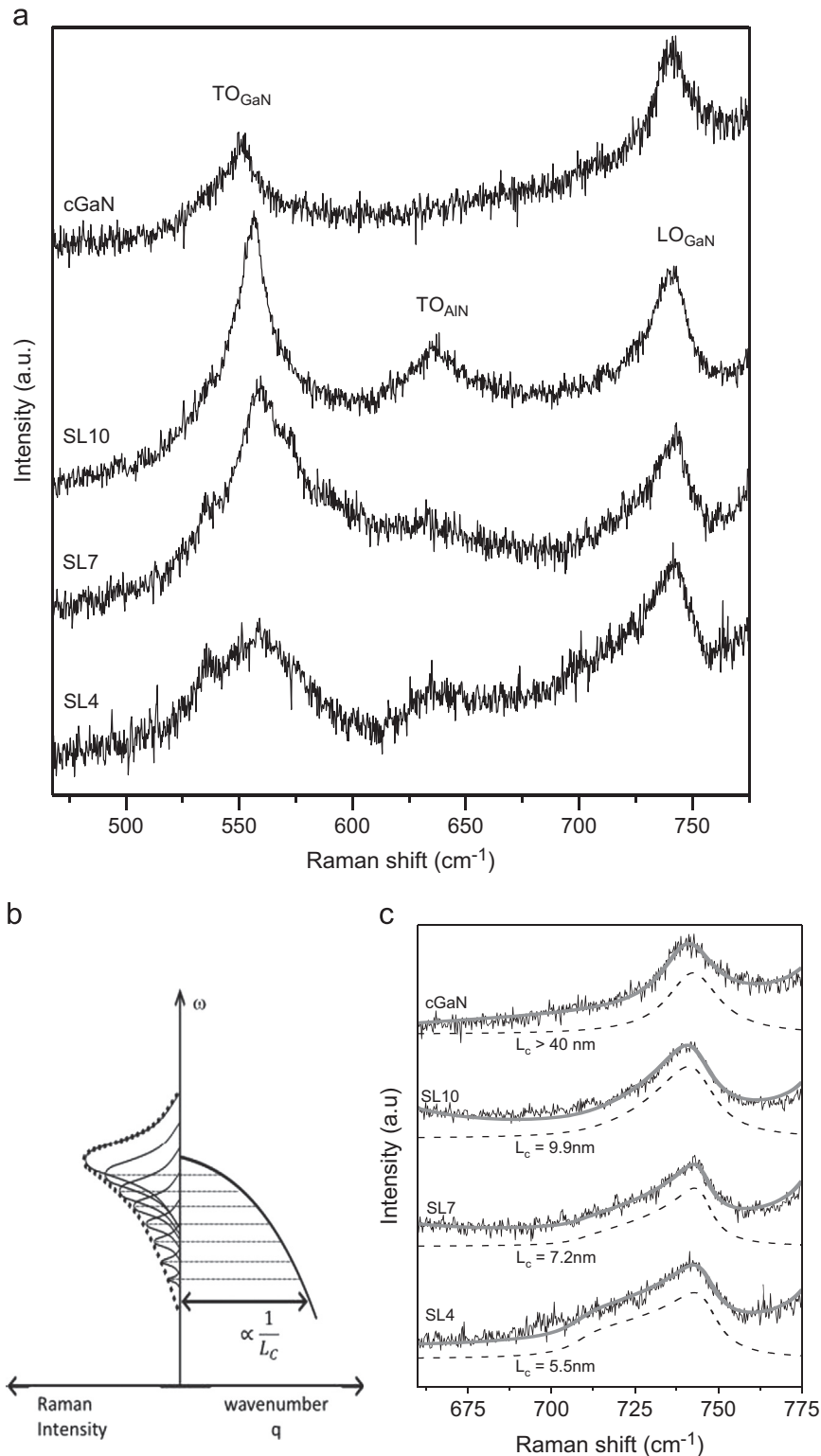
Fig. 3. (a) Raman spectra taken from bulk c-GaN and GaN/AlN superlattices with GaN thickness of 4, 7 and 10 nm and an AlN barrier thickness of 2 nm. (b) Schematic representation of the influence of the phonon localization effect in the Raman line shape. (c) Experimental (thin black lines) and calculated (gray lines) Raman spectra detailed in LO_{GaN} range. The dashed lines are components of the spectra, calculated using the spatial correlation model.

to those measured in the other samples (for SL7 the FWHM is 84 meV and for SL4 it is 114 meV at 10 K). We believe that for SL7 and SL10 the grown layers are thick enough to accommodate the substrate imperfections, resulting in a minimization of the interface irregularities. For this reason, the obtained lengths of the phonon localization are closer to the nominal well thicknesses, and the PL peaks measured in these superlattices are sharper than that presented by the SL4 sample.

4. Conclusions

High quality cubic AlN/GaN superlattices with 100 periods were grown by plasma-assisted MBE. By reciprocal space map from HRXRD an average strain of 2.0% is measured related to 3C–SiC substrate. Room and low temperature PL measurements show the quantum confinement of carriers and an increase of

FWHM for thinner well thickness. By means of a spatial correlation model, we have studied the localization length of GaN-like longitudinal phonons in the wells of such structures. The values determined for the superlattices with larger periods are in good agreement with the thicknesses of the layers in which they must be localized. In the lower limit of the superlattice with the shortest period, we have found that such phonons describe a localization length slightly larger than the well thickness. This can be explained by the presence of more prominent interface roughness in this sample, which also have produced a broader photoluminescence peak as compared to longer period superlattices. The upper limit of 40 nm is obtained for this model to determine phonon localization in cubic GaN/AlN superlattices. Our results suggest the better range to explore phonon localization on cubic GaN/AlN superlattices.

Acknowledgments

References

[1] H. Machhadani, M. Tchernycheva, S. Sakr, L. Rigutti, R. Colombelli, E. Warde, C. Mietze, D.J. As, F.H. Julien, Phys. Rev. B 83 (2011) 195301.

[2] C. Mietze, E.A. DeCuir, M.O. Manasreh, K. Lischka, D.J. As, Phys. Stat. Solidi C: Curr. Topics Solid State Phys. 8 (4) (2011) 1204.

[3] E. Tschumak, R. Granzner, J.K.N. Lindner, F. Schwierz, K. Lischka, H. Nagasawa, M. Abe, D.J. As, Appl. Phys. Lett. 96 (2010) 253501.

[4] M. Rajalakshmi, A.K. Arora, B.S. Bendre, S. Mahamuni, J. Appl. Phys. 87 (2000) 2445–2448.

[5] G. Belenky, M. Dutta, V.B. Gorfinkel, G.I. Haddad, G.J. Iafrate, K.W. Kim, M. Kisin, S. Luryi, M.A. Stroscio, J.P. Sun, H.B. Teng, S.G. Yu, Physica B 263 (1999) 462–465.

[6] C.Y. Sung, T.B. Norris, A. AfzaliKushaa, G.I. Haddad, Appl. Phys. Lett. 68 (1996) 435–437.

[7] M. Eric, V. Milanovic, Z. Ikonic, D. Indjin, Solid State Commun. 142 (2007) 605–609.

[8] J. Zhu, S.L. Ban, S.H. Ha, Chin. Phys. B 21 (2012) 097301.

[9] S.K. Medeiros, E.L. Albuquerque, G.A. Farias, M.S. Vasconcelos, D.H.A. L. Anselmo, Solid State Commun. 135 (2005) 144–149.

[10] A.B. Fu, M.R. Hao, Y. Yang, W.Z. Shen, H.C. Liu, Chin. Phys. B 22 (2013) 026803.

[11] V.Y. Davydov, E.M. Roginskii, A.N. Smirnov, Y.E. Kitaev, M.A. Yagovkina, R. N. Kyutt, M.M. Rozhavskaya, E.E. Zavarin, W.V. Lundin, M.B. Smirnov, Phys. Stat. Solidi a-Appl. Mater. Sci. 210 (2013) 484–487.

[12] J. Schörmann, S. Potthast, D.J. As, K. Lischka, Appl. Phys. Lett. 90 (2007) 041918.

[13] D.J. As, K. Lischka, in: M. Henini (Ed.), Molecular Beam Epitaxy: From Quantum Wells to Quantum Dots; From Research to Mass Production, Elsevier, ISBN 97801238783972013, p. 203, http://dx.doi.org/10.1016/B978-0-12-387839-7.00011-7.

[14] J. Schörmann, S. Potthast, D.J. As, K. Lischka, Appl. Phys. Lett. 89 (2006) 131910.

[15] I.H. Campbell, P.M. Fauchet, Solid State Commun. 58 (1986) 739–741.

[16] H.M. Tütüncü, S. Bagci, G.P. Srivastava, A.T. Albudak, G. Ugur, Phys. Rev. B 71 (2005) 195309.

[17] M.E. Twigg, B.R. Bennett, B.V. Shanabrook, J.R. Waterman, J.L. Davis, R. J. Wagner, Appl. Phys. Lett. 64 (1994) 3476–3478.